5

# Mountains and Midlatitude Aridity

*Anthony J. Broccoli and Syukuro Manabe*

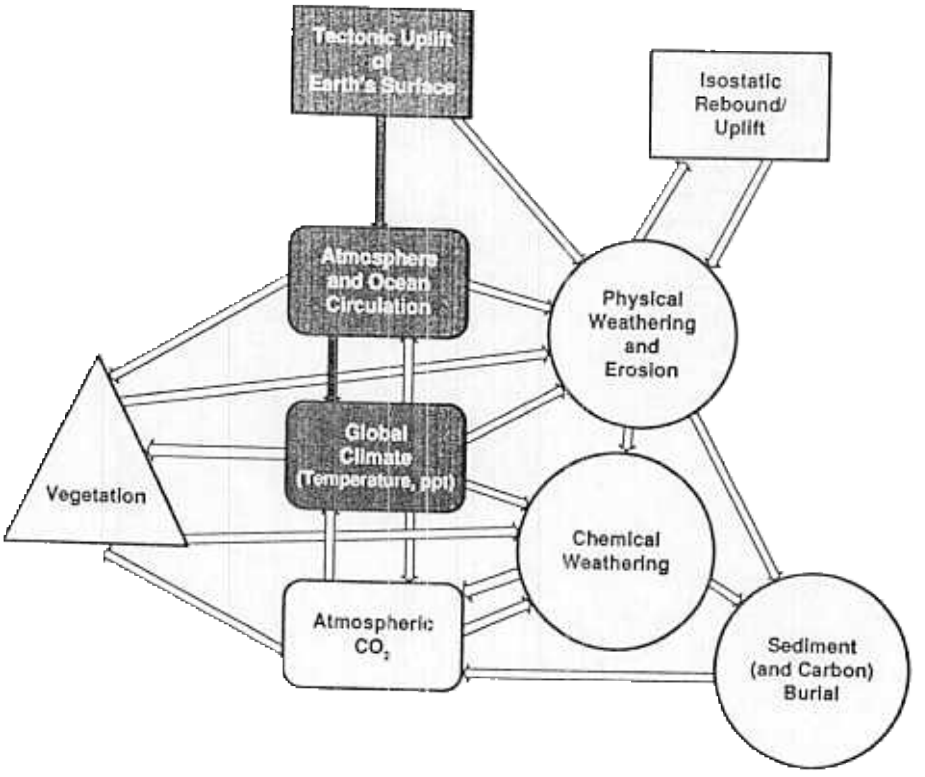


*Anthony J. Broccoli and Syukuro Manabe* • Geophysical Fluid Dynamics Laboratory/NOAA, Princeton University, Princeton, New Jersey 08542.

*Tectonic Uplift and Climate Change*, edited by William F. Ruddiman. Plenum Press, New York, 1997.

## 1. INTRODUCTION

The geological record provides evidence that suggests a link between mountain uplift and changes in climate over substantial regions of the world.[1] One approach to understanding the effect of mountain uplift on the evolution of climate is to investigate the role of present-day orography in determining the modern distribution of climates. A better understanding of the mechanisms by which the global distribution of mountains affects today's climate may shed light on the changes in climate that would occur in response to changes in orography. Unfortunately, even to understand the role of modern orography presents a difficult task that is not likely to be accomplished using observations alone, because the interaction among the many components of the climate system limits our ability to isolate mountain effects from other influences such as the location, size, and shape of the continents or the spatial distribution of incoming solar radiation.

To overcome this difficulty, numerical models of the Earth's climate can be employed to provide a framework in which it is possible to isolate the effects of mountains on the distribution of climate. They can be used to perform a controlled experiment in which climate is simulated with and without orography, just as scientists in other disciplines would conduct controlled experiments in the laboratory. Provided that the climate model is realistic enough to represent the relevant processes, results from such experiments may be expected to elucidate the mechanisms that operate in the real climate system. Thus climate modeling is a powerful tool for exploring the effects of orography on climate.

In this chapter we will present some recent results from a series of experiments using a climate model developed at the Geophysical Fluid Dynamics Laboratory (GFDL) of the National Oceanic and Atmospheric Administration.[2,3] These results indicate that the existence of midlatitude arid climates may be linked to the modern distribution of orography, making it possible that the geologically recent expansion of such dry regions is associated with mountain uplift.

## 2. DISTRIBUTION OF ARID CLIMATES

Most of the Earth's arid climates (i.e., those in which potential evapotranspiration exceeds precipitation on an annual basis) are found in the lower and middle latitudes. Widespread subtropical dry regions exist in northern Africa, the Middle East, Pakistan and northwestern India, the southwestern United States and Mexico, coastal Peru and Chile, southern Africa, and Australia. All of these regions lie in belts between 15° and 35° latitude on either side of the equator, and their existence is explained by their location beneath the subsiding branch of the Hadley circulation. But other sizable dry regions exist across the interior of Asia from Turkestan east to the Gobi Desert, in the western interior of North America

from the Great Basin to the prairies of Canada and the Great Plains, and east of the Andes in south central South America. These dry regions are not as readily explained by a simple schematic model of global circulation, since they are located beneath the traveling disturbances of the midlatitude westerlies.

Midlatitude aridity in the Northern Hemisphere is often explained by the large distance between oceanic moisture sources and the interiors of North American and Asia, with the dryness accentuated in some locations by the presence of mountain barriers upwind.[4-6] If distance from oceanic moisture sources is its primary cause, then midlatitude aridity (although perhaps less intense) would be expected even in the absence of orography. This hypothesis can be tested with atmospheric general circulation models (GCMs) using the methodology described in the introduction to this chapter.

## 3. REVIEW OF PREVIOUS CLIMATE MODELING WORK

In the early days of climate modeling, a number of studies were performed in which GCMs were used to simulate the Earth's climate with and without mountains.[7-11] Some information resulting from these and other studies hints at the possibility that midlatitude aridity may be related to the modern distribution of orography. In a paper that primarily concerned changes in the boreal wintertime atmospheric circulation, Manabe and Terpstra[10] briefly discussed the differences in precipitation distribution based on simulations of the January climate with and without mountains. They found a zonal belt of moderate precipitation stretching across the midlatitudes of the Northern Hemisphere in the case without mountains, and interruptions in this zonal belt over the interiors of Eurasia and North America in their experiment with mountains. In their investigation of the role of mountains in the south Asian summer monsoon circulation, Hahn and Manabe[11] found that the monsoon circulation was greatly altered in their experiment without mountains, and that the presence of the Tibetan Plateau was required for the northward expansion of the monsoon over India. Using realistic orography and incorporating seasonal variation, Manabe and Holloway[12] found that their model simulated the midlatitude dryness of the Eurasian interior. Based on the results of the winter simulations of Manabe and Terpstra[10] and the summer simulations of Hahn and Manabe,[11] they suggested that the Tibetan Plateau plays a major role in maintaining this dryness.

Interest in mountain effects on global circulation and climate resurfaced in the latter half of the 1980s.[13-15] Figuring prominently in this renewed interest was the suggestion that changes in climate during the past 30 to 40 million years may be associated with large-scale uplift of the Tibetan Plateau and the western United States.[16] Kutzbach *et al.*[15] used the Community Climate Model of the National Center for Atmospheric Research (NCAR CCM) to run perpetual January and July integrations with and without mountains in order to study changes in climate in both the summer and winter seasons. Substantial similarity

exists between their January results and those of Manabe and Terpstra,[10] as well as between the response of the model to changes in orography and climatic changes in the geological record.[16]

The remainder of this chapter will focus on the results obtained by Manabe and Broccoli[2] and Broccoli and Manabe[3] using the GFDL climate model. We will examine specifically the ability of the model to simulate midlatitude arid climates. We will also investigate the mechanisms, both atmospheric and hydrologic, by which those climates are maintained.

## 4. MODEL DESCRIPTION

The version of the GFDL climate model used in this study consists of two basic units: (1) a general circulation model of the atmosphere, and (2) a heat and water balance model over the continents. These components are fully interactive. To reduce the computational burden, these components are not coupled to an ocean model; instead, the geographical distribution of sea surface temperature and sea ice is prescribed, varying seasonally, in a manner consistent with observations.

The atmospheric model employs the spectral transform method, in which the horizontal distributions of the primary variables are represented by spherical harmonics. The present model retains 30 zonal waves, adopting the so-called rhomboidal truncation. The spacing of the transform grid is 2.25° latitude by 3.75° longitude. Normalized pressure is used as the model's vertical coordinate, with nine unevenly spaced levels used for finite differencing. Gordon and Stern[17] provide further discussion of the dynamical component of this model.

Solar radiation at the top of the atmosphere is prescribed, varying seasonally but not diurnally. Computation of the flux of solar radiation is performed using a method similar to that of Lacis and Hansen,[18] except that the bulk optical properties of various cloud types are specified. Terrestrial radiation is computed as described by Stone and Manabe.[19] For the computation of radiative transfer, clouds are prescribed, varying only with height and latitude. The mixing ratio of carbon dioxide is assumed constant everywhere, and that of ozone is specified as a function of height, latitude, and season.

Over the continents, surface temperatures are computed from a heat balance with the requirement that no heat is stored in the soil. Both snow cover and soil moisture are predicted. A change in snow depth is predicted as the net contribution from snowfall, sublimation, and snowmelt, with the latter two determined from the surface heat budget. Soil moisture is computed by the "bucket method." The soil is assumed to have a water-holding capacity of 15 cm. If the computed soil moisture exceeds this amount, the excess is assumed to be runoff. Changes in soil moisture are computed from the rates of rainfall, evaporation, snowmelt, and runoff. Evaporation from the soil is determined as a function of soil moisture and the potential evaporation rate (i.e., the hypothetical evaporation rate from a completely wet soil). Further details of the hydrologic computations can be found in Manabe.[20]

An additional characteristic of the model is a parameterization of the drag that results from the breaking of orographically-induced gravity waves. Parameterizations of this kind have been found to improve the performance of atmospheric GCMs both for weather forecasting and climate simulation.[21,22] In the current experiments, gravity wave drag is used in all integrations where orography was present, and it substantially improves the simulation of midlatitude aridity. A description of this parameterization and a discussion of its impact on the simulation of climate are contained in Appendix A of Broccoli and Manabe.[3]

## 5. EXPERIMENTAL DESIGN

Three numerical integrations are run with the model as described in the previous section. In the first of these, the mountain (M) integration, realistic geography and topography are used as depicted in Fig. 1. Because topography in a spectral model must be represented mathematically by a finite series of spherical harmonics, it is relatively smooth. Despite this smoothness, most of the large-scale features of the global topography are represented, such as the Tibetan Plateau, the Rocky and Andes cordilleras, the east African highlands, and the Greenland and Antarctic ice sheets. A second integration, the no-mountain (NM) integration, uses the same geographical distribution of land and sea as the M integration, but with flat continents. Comparing the results from these two integrations provides the response of the climate system (as represented by the model) to the presence of orography. A wide variety of interactions or feedbacks is included in the model, and thus the response takes into account the effects of these interactions. A third integration, known as the fixed soil moisture (FSM) integration, is performed to evaluate one of these feedbacks, specifically that between the land surface and the atmosphere. The FSM integration is identical to the M integration except that the soil moisture value at each gridpoint is prescribed, varying seasonally, rather than predicted from a water balance. (The soil moisture values are based on the climatological values from the NM integration using the procedure employed by Delworth and Manabe[23] in their prescribed soil moisture experiment.) By utilizing the results from the FSM integration, it is possible to determine to what extent the interaction between the land surface and the atmosphere enhances the mountain-induced changes in climate.

All integrations were initiated from an isothermal, resting atmosphere and integrated until the simulated seasonal cycle of climate reached a quasi-equilibrium. Even though this initial state is very unrealistic, the atmospheric component of the model quickly adjusts and loses its memory of the initial conditions. Since sea surface temperature and sea ice were prescribed, no thermal adjustment of the ocean temperature was required, so only a relatively short spin-up period of several years was required for quasi-equilibrium to occur. A period of 3 years subsequent to the achievement of quasi-equilibrium was retained for analysis, and

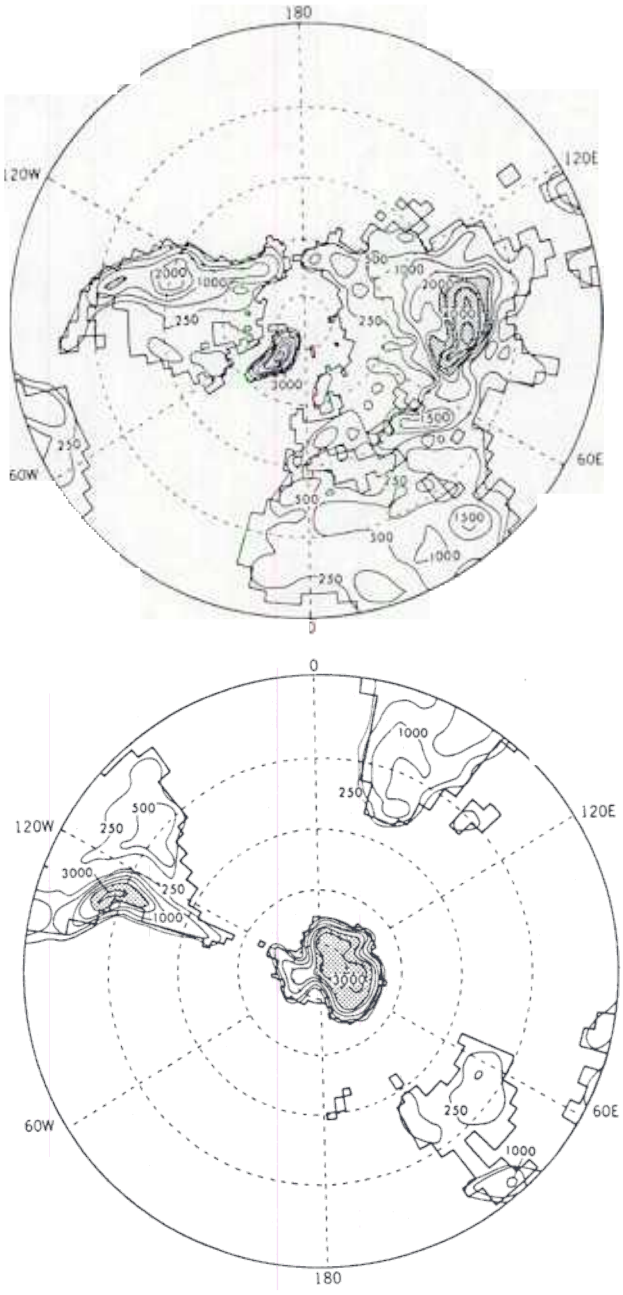


FIGURE 1. Surface elevation (m) of topography used for the M integration: (Top) Northern Hemisphere. (Bottom) Southern Hemisphere. Stippled areas indicate elevations >2000 m. Contours at 250, 500, 1000, 1500, 2000, 3000, 4000, and 5000 m. Owing to spectral truncation, contours extend over oceans as model elevation is not constrained to be zero at ocean gridpoints.

the results presented herein utilize data from those 3-year periods unless otherwise noted.

## 6. SIMULATED DISTRIBUTION OF DRY CLIMATES

The climate model output is used to determine the Köppen climate classification at each gridpoint for the M and NM integrations. Climate classification systems such as this are useful, albeit arbitrary, in providing an indication of the overall character of the simulated climates. In the Köppen system, monthly mean temperature and precipitation are used to classify climate in a manner intended to correspond to the prevailing natural vegetation. The Köppen scheme is a commonly used climate classification that has been used previously to examine climates simulated by GCMs.[12,24] A detailed description of the Köppen scheme can be found, for example, in Lamb.[25]

Köppen category B denotes desert and steppe climates, where precipitation is insufficient to meet the demands of forest vegetation at the prevailing temperatures. The spatial distributions of the B climates simulated by the M and NM integrations are compared to the observed distribution in Fig. 2. In the NM integration, dry climates are confined to zonal (or east–west) belts between 15° and 35° latitude in each hemisphere. These subtropical belts of aridity are nearly continuous, with only the southeastern parts of Asia and North America experiencing more moist climates. Midlatitude dryness is almost completely absent in the NM integration. This contrasts sharply with the results from the M integration, in which the subtropical dry regions are not as extensive and Köppen's category B climates occur across the midlatitude interior of Eurasia and, to a lesser extent, North America. Comparison with the observed distribution indicates that the M integration is in good agreement over the midlatitude Northern Hemisphere, implying that the model's simulation of temperature and precipitation in these regions is realistic.

The geographical distribution of annual mean soil moisture (Fig. 3) provides another measure of model aridity. In the NM integration, little east–west variation of soil moisture occurs, although the east coasts of North America and Asia are somewhat wetter than the remainder of those continents (as noted in the distribution of B climates). The pattern of soil moisture contours in the NM integration is largely zonal, with values in excess of 80% of saturation along the northern coasts of the continents and below 20% in the subtropics. This zonal symmetry is not present in the M integration, in which substantial east–west variation exists across both Eurasia and North America. Of particular interest to this study are two midlatitude regions of soil dryness. One extends eastward from the Caspian Sea across central Asia into northwest China, while another lies just east of the Rocky Mountains in Canada and the northern United States.

There is a great deal of similarity between the areas of low soil moisture and the regions where Köppen's category B climates are simulated. The reason for this

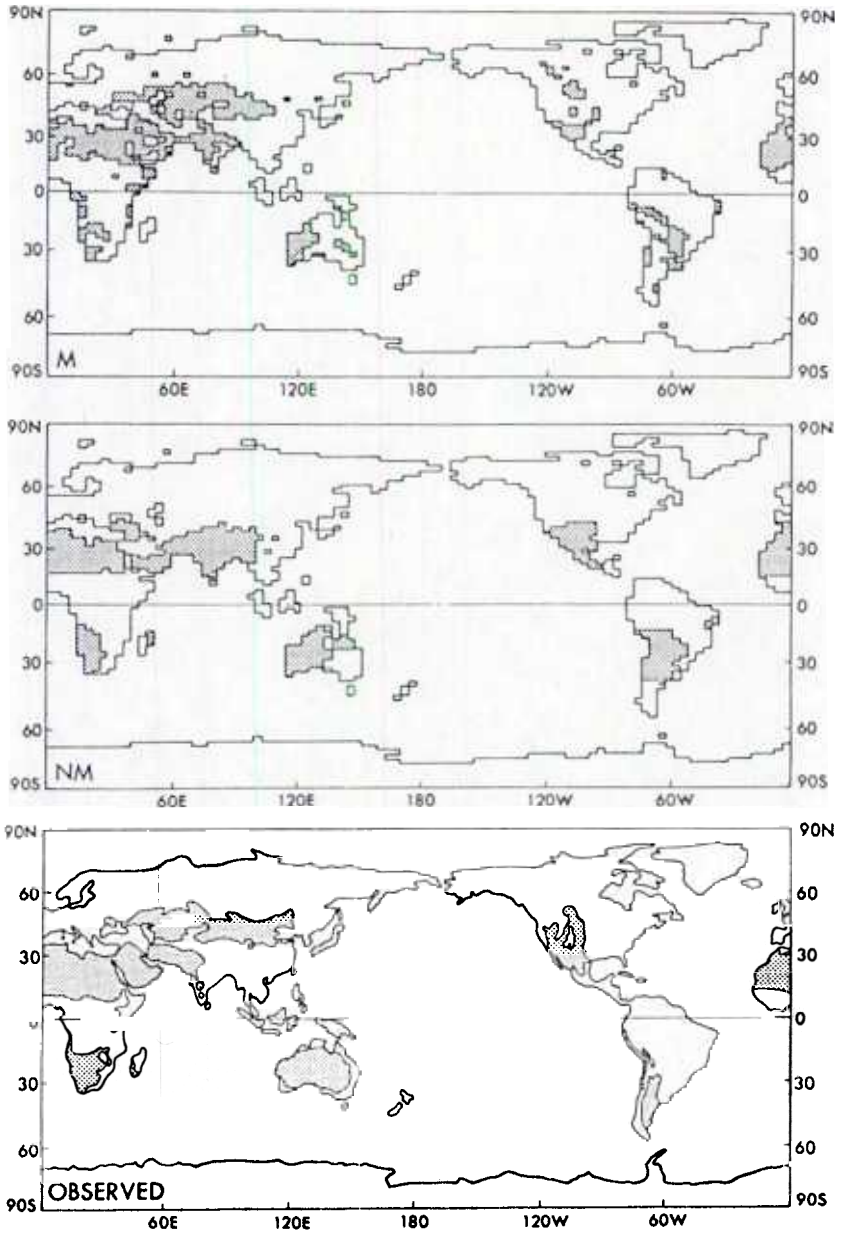


FIGURE 2. Distribution of arid and semiarid climates (indicated by stippling) according to the Köppen climate classification: (Top) M integration. (Center) NM integration. (Bottom) Observed.

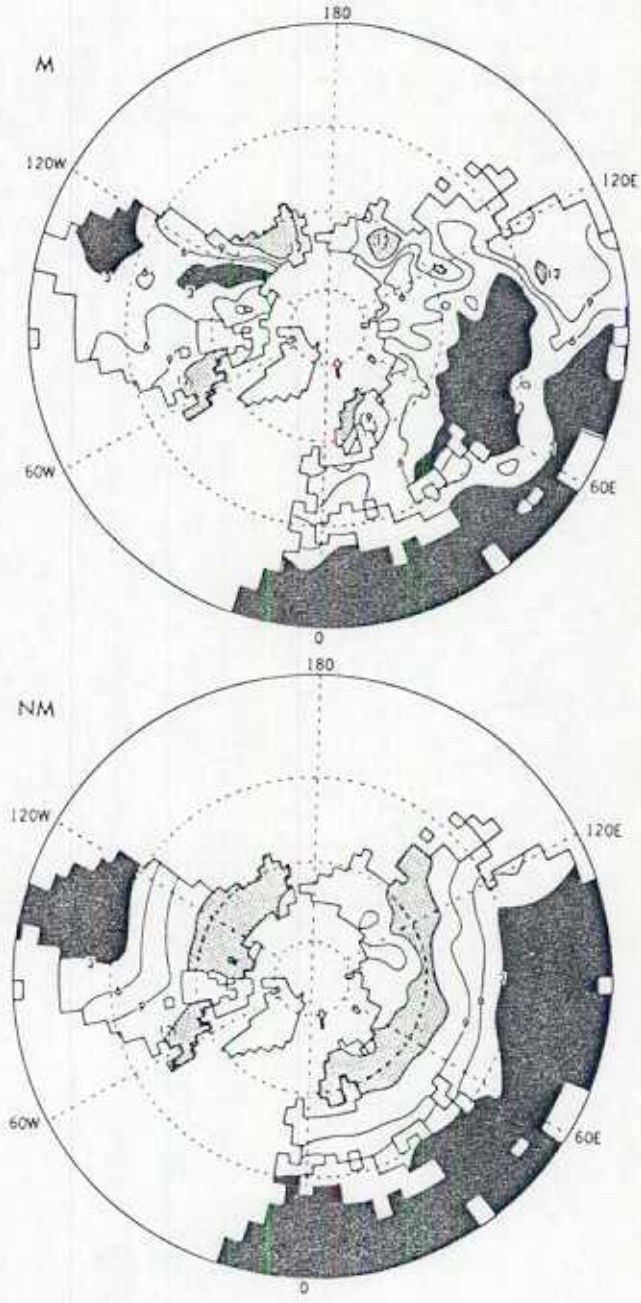


FIGURE 3. Annual mean soil moisture (cm): (Top) M integration. (Bottom) NM integration. Stippling indicates soil moisture >12 cm; solid black indicates soil moisture <3 cm. The field capacity of soil moisture in both integrations is 15 cm everywhere. A 1-2-1 smoothing has been applied in both directions to reduce grid scale variability.

similarity is evident when the method of computation of the Köppen classification is compared with the hydrologic component of the climate model. The Köppen scheme classifies arid and semiarid climates on the basis of an empirical relationship involving temperature and precipitation, using temperature as a surrogate for the potential evaporation from the land surface. The B climates are those in which potential evaporation substantially exceeds precipitation. In the climate model, a balance must exist (on an annual mean basis) between the inflow to the soil moisture "bucket" (precipitation) and the outflow (evaporation and runoff). The evaporation $E$ is related to the potential evaporation $E_p$ by $E = \beta E_p$, where $\beta = \min(w/w_k, 1.0)$, with $w$ the soil moisture and $w_k$ an empirical value (chosen to be 11.75 cm, or 75% of field capacity) below which evaporation is limited by soil moisture. The potential evaporation is determined from a surface heat budget, and is thus positively correlated with temperature. Thus for $w < w_k$, the actual evaporation is smaller than the potential evaporation by a factor of $w/w_k$. Given the balance requirement between precipitation and evaporation (if runoff is assumed to be small), this implies that potential evaporation exceeds precipitation wherever $w < w_k$. Thus the regions where soil moisture is well below the critical value ($w_k$) of 75% of field capacity experience potential evaporation that greatly exceeds precipitation.

The contrast between the largely zonal pattern of the NM integration and the more complex pattern of the M integration that appears in the Köppen classification and soil moisture distributions is also present for annual mean precipitation (Fig. 4). Without orography, precipitation is lightest over the Arctic Ocean and in two subtropical regions: southwestern North America and the adjacent Pacific, and northern Africa and the nearby Atlantic. Precipitation is relatively heavy in a band that circles the hemisphere between 45° and 65°N, and also at lower latitudes over the western North Atlantic and western North Pacific. In the M integration, more east–west variability occurs at midlatitudes than in the NM integration, and precipitation is light over the same continental interior regions where soil moisture is low. Annual precipitation rates of less than 1 mm/day extend across central Asia and in a band just east of the Rocky Mountains in North America.

Three regions (outlined in Fig. 5) were selected for more detailed analysis: west central Asia, east central Asia, and the Canadian prairie. To explore the seasonal variations of the difference in precipitation between the M and NM integrations, the annual cycle of precipitation is computed for each of these regions (Fig. 6). In all three areas, precipitation in the M integration is substantially lower than in the NM integration throughout the entire year. The seasonal cycles of precipitation for the M integration are somewhat different in each region, with a late winter/early spring maximum in west central Asia, a summer maximum in east central Asia, and a spring maximum in the Canadian prairie. In the NM integration, the heaviest precipitation in all three regions occurs during the period March through June, with a secondary autumn maximum in west central Asia and the Canadian prairie. Although there is some disagreement between the annual march of precipitation from the M integration and the

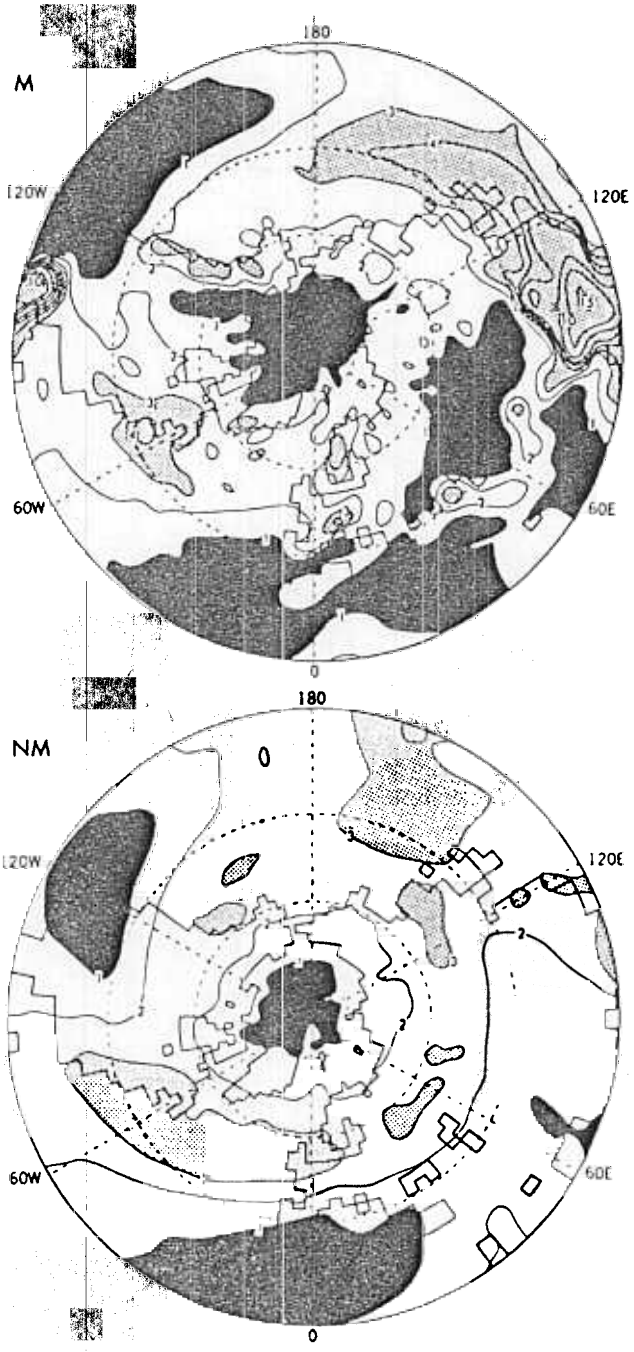


FIGURE 4. Annual mean precipitation (mm/day): (Top) M integration. (Bottom) NM integration. Contours at 1, 2, 3, 4, 5, 6, 8, 10, 15, 20, 30 mm/day. Smoothing as in Fig. 3.

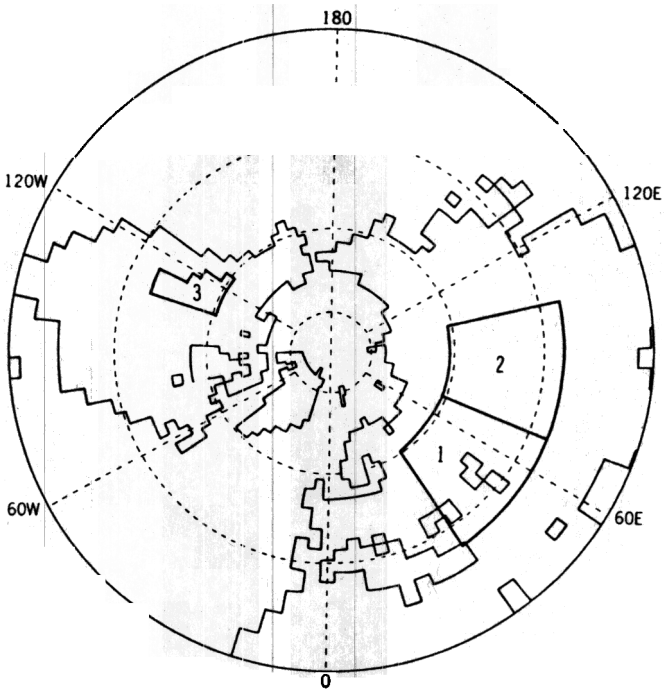


FIGURE 5. Areas used in computation of regional precipitation: (1) west central Asia; (2) east central Asia; (3) Canadian prairie. Only land points within these regions were used in the computations.

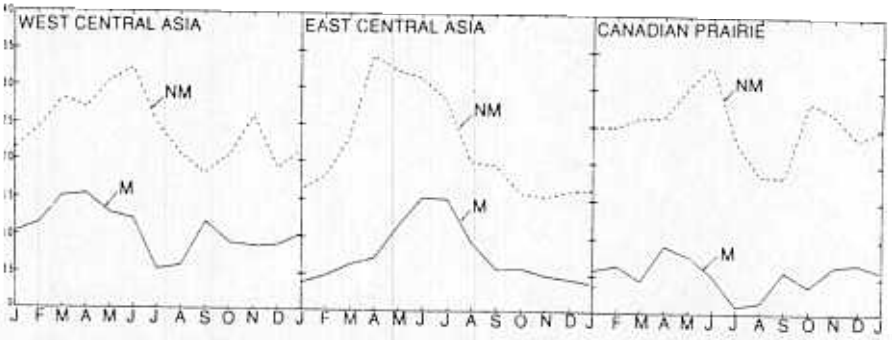


FIGURE 6. Seasonal variation of monthly precipitation (mm/day) from the M and NM integrations for three regions: (Left) west central Asia. (Center) east central Asia. (Right) Canadian prairie.

observed precipitation climatology for west central Asia and the Canadian prairie, these differences are generally small when compared to the differences between the M and NM integrations.

## 7. LARGE-SCALE ATMOSPHERIC CIRCULATION

A substantial decrease in both soil moisture and precipitation is simulated over portions of the interiors of Eurasia and North America in response to the modern distribution of orography. How do mountains alter the atmospheric circulation to produce this drying? A relatively simple and well-understood mechanism probably contributes to the dryness of the western interior of North America. As the prevailing westerly winds in the lower troposphere encounter the Rocky Mountains, air is forced upward. The reduction of pressure as the air ascends results in a cooling, so that much of the moisture contained in the air condenses to form clouds and precipitation. Once the air crosses the highest elevations and starts downward, the increasing pressure warms the moisture-depleted air. (The well-known chinook winds of the Rocky Mountain foothills result from a similar mechanism on a smaller scale.) The ascending moist air on the upwind side results in orographic precipitation, while the subsiding dry air on the downwind side inhibits precipitation. Although this so-called rainshadow effect plays an important role in the dryness of interior North America, it cannot satisfactorily explain the extensive dryness of central Asia, as that continent lacks an extensive meridional barrier such as the Rocky Mountains. Other mechanisms must be involved in maintaining the arid climate of the Eurasian interior, and these mechanisms contribute to the dryness of western interior North America as well.

To identify one such mechanism, consider the processes responsible for the precipitation that falls in midlatitudes. Much of this precipitation is associated with the passage of transient disturbances (i.e., extratropical cyclones) with timescales of about 3–5 days. As discussed extensively by James,[26] such disturbances are not uniformly distributed throughout the midlatitudes of the Northern Hemisphere. Instead, they tend to be organized along "storm zones" or "storm tracks" that extend across the North Pacific and North Atlantic oceans. These locations have a specific relationship to the preferred positions for waves in the upper-tropospheric westerlies that become evident when the circulation is averaged over time periods of many seasons. The major storm tracks parallel the upper-tropospheric jet streams that occur between the prominent cold season stationary trough axes over eastern Asia and eastern North America and their corresponding downstream ridges.[27–29]

Theoretical studies[30,31] have linked the positions of these stationary waves to the spatial distribution of the underlying topography, with the ridge position (anticyclonic flow) in the vicinity of the topographic ridge and the trough position (cyclonic flow) downstream. Using a steady linear primitive equation model, Nigam *et al.*[32] found that orographic forcing was responsible for about two-thirds

of the overall amplitude of winter stationary waves in the upper troposphere in the Northern Hemisphere. Thus it can be argued that mountains may contribute to the existence of midlatitude dry regions by inducing stationary waves that largely determine the favored locations for extratropical disturbance activity. If this argument is correct, there should be a clear relationship between the distribution of midlatitude precipitation and stationary wave position. This hypothesis can be evaluated by examining the simulated atmospheric circulation from the M integration and comparing it to the corresponding circulation features in the NM integration.

The large seasonal changes in climate that occur in the midlatitude Northern Hemisphere require an examination of the entire seasonal cycle of precipitation and circulation. To facilitate this approach, longitude–time sections have been constructed by computing meridional averages of precipitation and 500-mb geopotential height for the belt from 30°–50°N. The 500-mb geopotential height is used to depict the atmospheric circulation, as winds at this level (to a close approximation) blow parallel to the geopotential height contours, with lower heights to the left. The geopotential height is expressed as a departure from the zonal mean to emphasize the seasonal variations in the position of stationary waves and eliminate the large thermally induced seasonal cycle in zonal mean geopotential height. Troughs and ridges appear as relative minima and maxima, respectively.

The longitude–time section for the M integration (Fig. 7, left) indicates the existence of waves that maintain an almost constant longitude for substantial portions of the seasonal cycle. Of most importance to this study are the ridge–trough couplets that occur over North America through most of the year and the eastern half of Eurasia during the cold season, with the trough axes along or just east of the east coasts of these continents. (Note that the Tibetan Plateau and Rocky Mountains are at longitudes of 75–100°E and 240–255°E, respectively.) For each of these features, the heaviest precipitation tends to occur along and just east of the trough axis, with much lighter precipitation occurring upstream in the vicinity of and just downstream of the ridge. This is consistent with the hypothesis, based in part on theoretical studies of the wintertime Northern Hemisphere circulation, that orographically induced stationary waves organize the distribution of midlatitude precipitation and contribute to the existence of midlatitude dry regions.

In the warm season there is a substantial weakening and westward shift of the east Asian trough as the Asian monsoon circulation becomes a more dominant influence. This is accompanied by a corresponding westward shift in both the wet and dry regions. In contrast, there is very little evidence of a similar circulation change over North America, as expected given the absence of a strong monsoon circulation there.

The stationary waves from the NM integration (Fig. 7, right) have much smaller amplitude and less seasonal persistence than those of the M integration. Although the precipitation distribution in the NM integration is not perfectly uniform, it is much more amorphous and lacks the relationship to the stationary

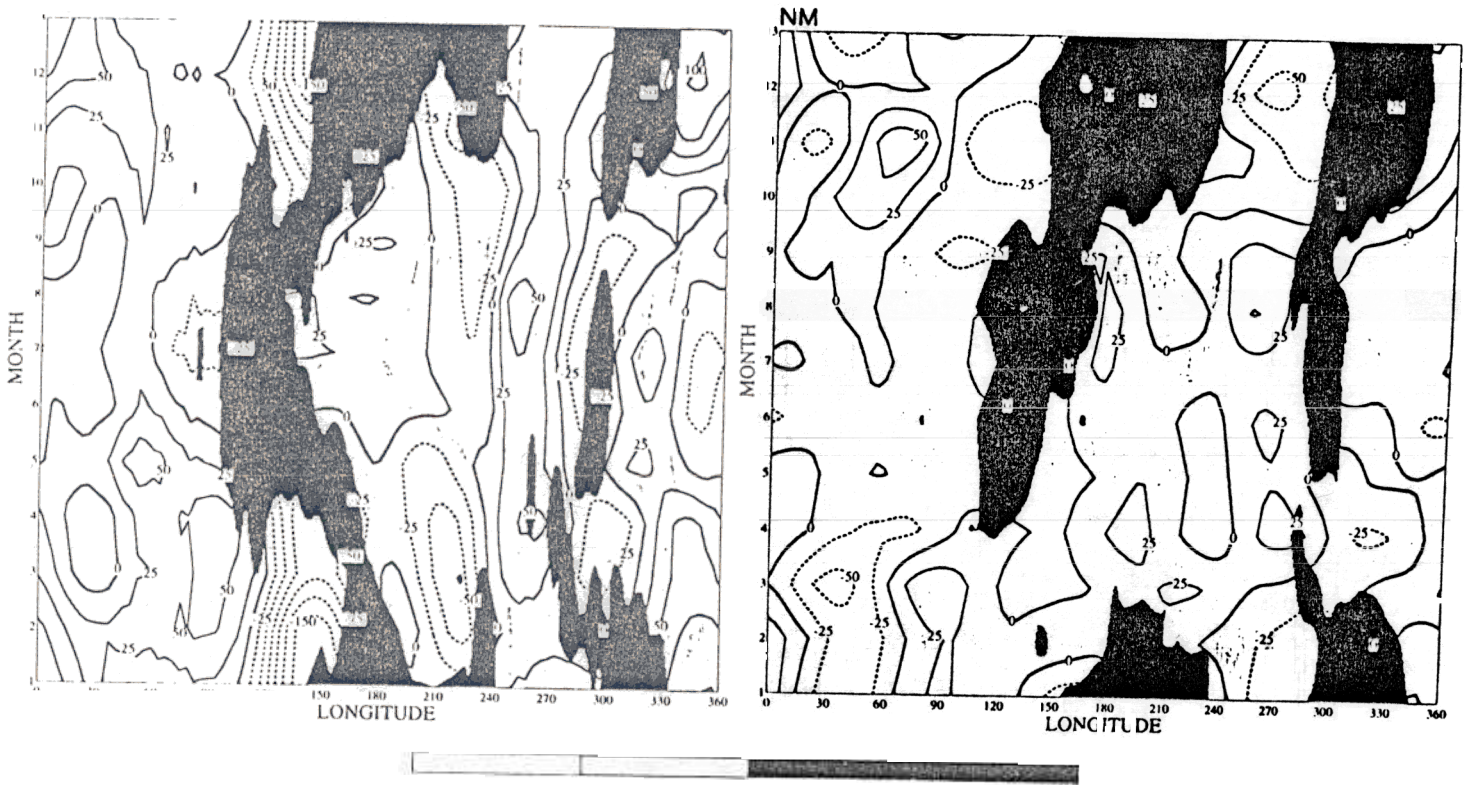


IGURE 7. Longitude–time section of 500-mb geopotent and precipitation (mm/day; indicated by shading averaged 75–100°E and 240–255°E, respectively

height departure from zonal mean, m; indicated by contours with negative contours dashed) om 30° to 60°N. For reference, the Tibetan Plateau and Rocky Mountains are at longitudes

wave pattern that is so prominent in the M integration. The absence of midlatitude dryness over the continents is evident from the reduction in the prominence of the unshaded regions, indicative of precipitation rates less than 1 mm/day. There remains some tendency for the oceans to be wetter than the continents in winter, and for the east coasts of the continents to be wetter than the west coasts in summer.

To further examine the relationships between circulation and precipitation in the M and NM integrations, a more detailed examination is warranted. Because the longitude–time section from the M integration provides evidence of important seasonal changes, particularly over Eurasia, the examination will focus on the boreal winter and summer seasons.

### 7.1. Winter

Various diagnostics of the atmospheric circulation at the 500-mb level (i.e., 5–6 km above sea level) are used to examine the circulation in boreal winter (December–January–February). The stationary waves can be seen as the meandering of the 500-mb geopotential height contours. Isotachs, or contours of wind speed, enable the identification of jet streams, and the root-mean-square (rms) of the daily geopotential height (band-pass-filtered to retain fluctuations with timescales between 2.5 and 6 days) provides a measure of storminess. The 500-mb level is chosen as Blackmon *et al.*[29] and Blackmon and Lau[33] have found that the rms of band-pass-filtered heights at that level corresponds well with synoptic-scale disturbances. While higher tropospheric levels may be equally or more suitable for identifying the stationary wave pattern and jet stream locations, comparison of upper tropospheric maps with those from the 500-mb level suggests that the features are similar.

When compared to the NM integration, the amplitude of the stationary waves in the M integration is substantially larger, as noted earlier from the longitude–time sections. The geopotential heights and isotachs (Fig. 8, top) from the NM integration follow a nearly circular pattern, with only low-amplitude waves and a circumpolar jet axis centered between 45° and 50°N. In contrast to this zonally symmetric picture, stationary waves are present in the M integration with troughs situated downstream of the Tibetan Plateau and Rocky Mountains. Each of these troughs is associated with a wind maximum located downstream, a feature simulated by Bolin[30] and Cook and Held[34] in response to idealized topography. The increase in the amplitude of stationary waves in the presence of orography is similar to that found by Manabe and Terpstra[10] and Kutzbach *et al.*[15]

Contrasting patterns between the M and NM integrations also appear in the rms of band-pass-filtered 500-mb heights (Fig. 8, center). In the NM integration, storminess is high in a circumpolar band between 40° and 60°N, nearly coincident with the maximum 500-mb winds. In the M integration, the bands of high storminess are more narrowly confined to maxima stretching across the North Pacific and North Atlantic. These storm tracks closely parallel the 500-mb wind

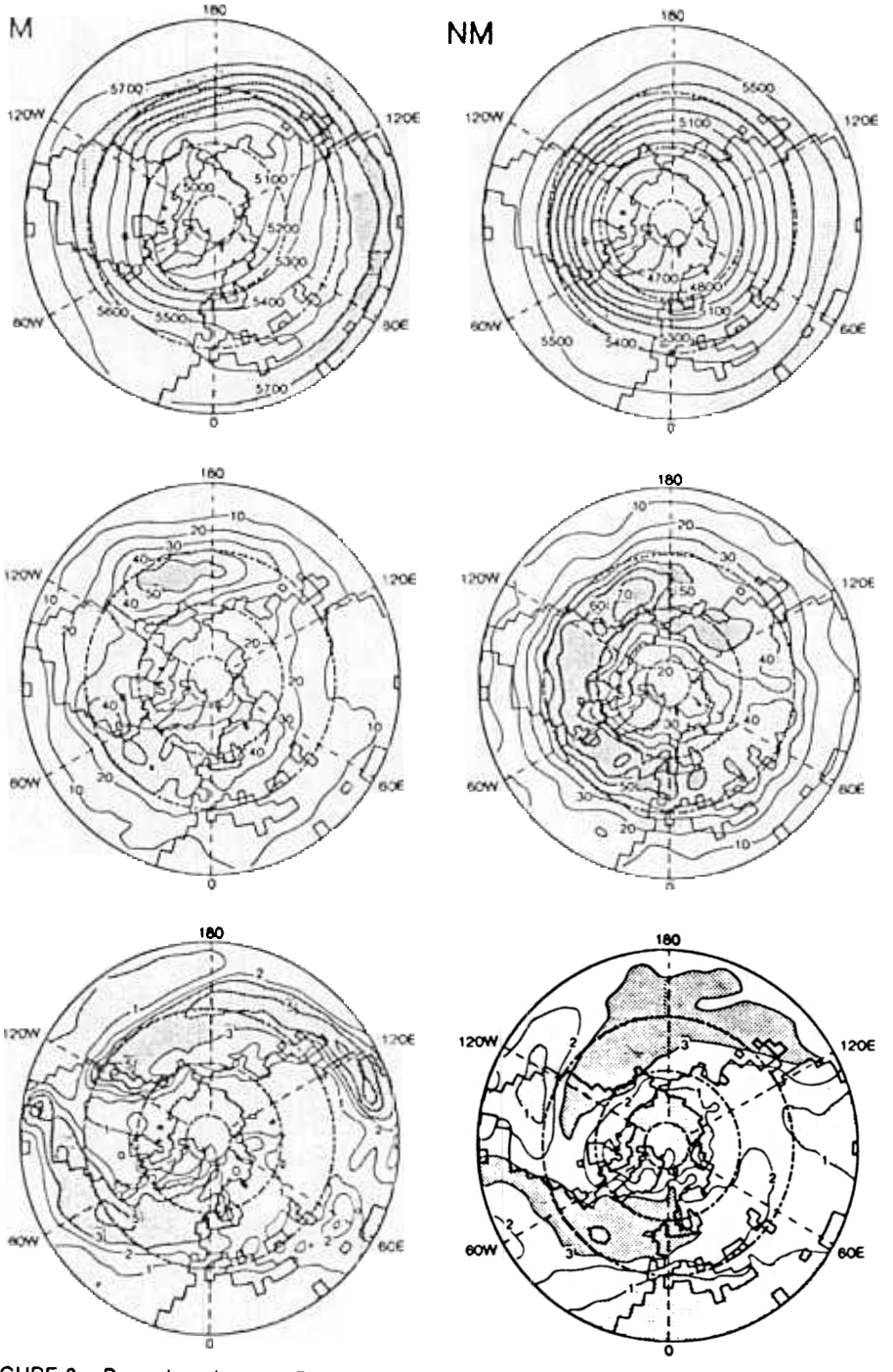


FIGURE 8. December-January-February circulation and precipitation from the (left) M integration and (right) NM integration: (Top) 500-mb geopotential height (dm). Light stippling indicates 500-mb winds > 15 m/s; dense stippling > 25 m/s. (Center) Root-mean-square (rms) of band-pass-filtered 500-mb geopotential height (m). The bandpass filter selects disturbances between 2.5 and 6 days. Light stippling indicates values > 30 m; dense stippling > 50 m. (Bottom) Precipitation (mm/day). Light stippling indicates precipitation < 1 mm/day; dense stippling > 3 mm/day. Contour interval as in Fig. 4, and smoothing as in Fig. 3.

speed maxima that occur downstream of the trough axes, in a relationship very similar to observations.[28] An association between storm tracks and jet axes is expected owing to the relationship between vertical wind shear and storm development, also noted by Manabe and Terpstra[10] in their GCM simulation. Substantially lower rms values occur over the regions of midlatitude aridity in the M integration than in the same locations in the NM integration, indicating a reduction in synoptic disturbance activity.

To see the relationship between precipitation and these circulation features, the bottom of Fig. 8 contains maps of winter precipitation from the M and NM integrations. There is some similarity between these distributions and their annual mean counterparts (Fig. 4). A zonal band of moderate precipitation ($\sim$2–3 mm/day) is evident over the continents between 40° and 60°N in the NM integration, with the heaviest amounts (>3 mm/day) over the western continental midlatitudes. This rain belt nearly coincides with the axis of maximum 500-mb winds and storminess. Elsewhere, the tendency for winter precipitation to be heavier over the oceans is also apparent, as discussed earlier in this section. In the M integration, much larger spatial variations occur in middle latitudes, with precipitation rates less than 1 mm/day east of the Canadian Rockies and across a vast region in eastern and central Asia. Precipitation over these regions is as little as one-third of that in the NM integration. Much heavier amounts of more than 4 mm/day occur over southeastern portions of Asia and North America near the western ends of the oceanic storm tracks.

The circulation maps further support the relationship between midlatitude precipitation and stationary waves during boreal winter that was evident in the longitude–time section from the M integration. Precipitation tends to be heaviest in the areas downstream of the stationary wave troughs, such as from the east coast of North America east–northeastward across the North Atlantic, and from China across Japan into the North Pacific. These regions of heavy precipitation are associated with high synoptic disturbance activity and relatively strong midtropospheric winds. In areas upstream of the troughs, synoptic disturbance activity is relatively weak and precipitation is light. In the more zonally symmetric NM integration, stationary wave amplitudes are small, so that precipitation and disturbance activity are associated with a circumpolar jet axis that is continuous around the hemisphere.

### *7.2. Summer*

The 500-mb circulation in the NM integration maintains its generally zonal character during boreal summer (Fig. 9, right). Although the associated jet stream is not as prominent, synoptic disturbance activity continues at a moderate level in a circumpolar belt between 40° and 60°N. The midlatitude rainbelt associated with these features is quite prominent over the continents, and is located toward the poleward side of this belt. Summer also brings relatively heavy rainfall at lower latitudes over the east coasts of North America and Asia. These are regions that lie under southerly surface flow on the west side of the oceanic

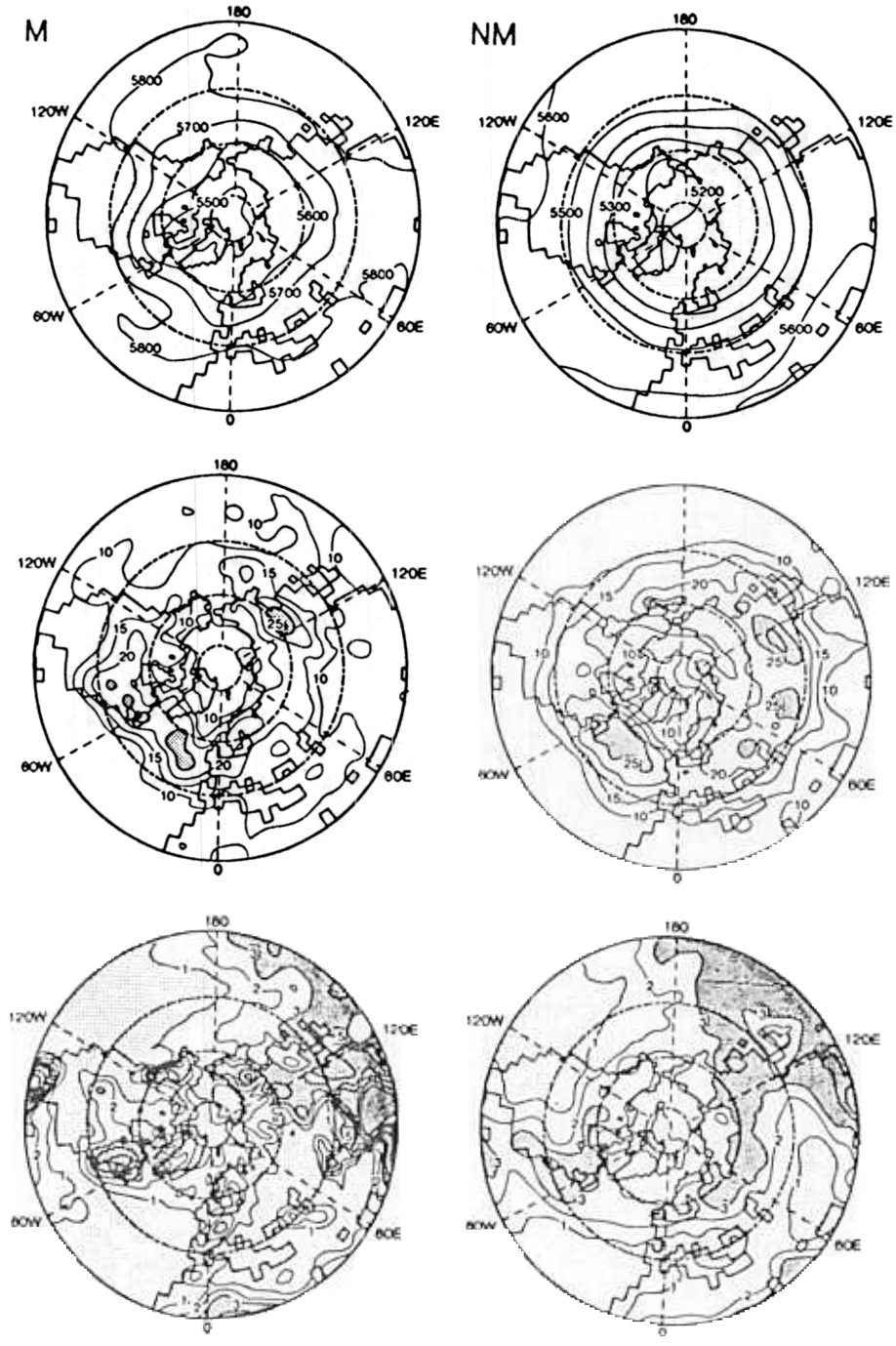


FIGURE 9. June-July-August circulation and precipitation from the (left) M integration and (right) NM integration: (Top) 500-mb geopotential height (dm). Light stippling indicates 500-mb winds >15 m/sec; dense stippling >25 m/sec. (Center) Root-mean-square (rms) of band-pass-filtered 500-mb geopotential height (m). The band-pass filter selects disturbances between 2.5 and 6 days. Stippling indicates values >25 m. (Bottom) Precipitation (mm/day). Light stippling indicates precipitation <1 mm/day; dense stippling >3 mm/day. Contour interval as in Fig. 4, and smoothing as in Fig. 3.

subtropical anticyclones, which reach their northernmost latitudes during the season.

In contrast to the NM integration, summer brings substantial changes to the stationary wave pattern in the M integration (Fig. 9, left), in terms of both wave amplitudes and positions, as discussed earlier in conjunction with the longitude–time sections. While a trough remains over eastern North America, the east Asian trough is not present. This is probably a consequence of the seasonal retreat of the westerlies, which are now far enough north that they no longer encounter the Tibetan Plateau. Despite this change, extensive dryness still prevails over central Asia, particularly west of 100°E, where the axis of a weak trough is located. The absence of this trough in the NM experiment suggests that it is the result of orographic forcing, either direct or indirect. The summer precipitation difference between the M and NM integrations in this region is substantial, with much drier conditions prevailing in the M experiment.

Previous work points to changes in the south Asian monsoon, the dominant circulation over much of the Asian continent in boreal summer, as a possible source of the reduction in summer precipitation over central Asia. In their GCM simulations with and without orography, Hahn and Manabe[11] found that mountains played a large role in the south Asian monsoon. They found that a center of rising motion was present above the Tibetan Plateau and its southern slope in the integration with mountains, but absent from the same location in the integration without mountains. Their result suggests that some of the differences in central Asian summer precipitation between the NM and M integrations could be due to the changes in the monsoon circulation.

Rising motion in the atmosphere is generally associated with the convergence of air in the lower troposphere and a corresponding divergence at upper levels. The irregularity of the surface often creates small-scale circulations that make it difficult to diagnose low-level convergence, so upper-level divergence is frequently used as an indication of the large-scale circulation. One way of diagnosing the upper-level divergence is to compute the velocity potential, as the divergent component of the flow is along the gradient of velocity potential. Thus a minimum (maximum) in the velocity potential is associated with large-scale divergence (convergence) at that level. The velocity potential at the 205-mb level (an altitude of $\sim 12$ km) from the NM integration (Fig. 10, center) indicates a very large-scale dipole pattern, with an elongated minimum over the western tropical Pacific and southeast Asia and a maximum over the tropical Atlantic. The heavy precipitation falling from southeast Asia eastward along the equatorial region suggests the importance of the latent heat of condensation in maintaining the upward vertical motion associated with this circulation. A similar dipole pattern is also present in the M integration (Fig. 10, top), but the primary center of the elongated minimum is shifted west-northwestward to southeast Asia, where precipitation is very heavy. In the difference map (Fig. 10, bottom) a strong center of negative values is located above the southeast portion of the Tibetan Plateau, indicative of increased upper divergence at that location. An area of enhanced precipitation coincides with this center, consistent with the orographically induced enhancement of the south Asian monsoon first noted by Hahn and Manabe.[11]

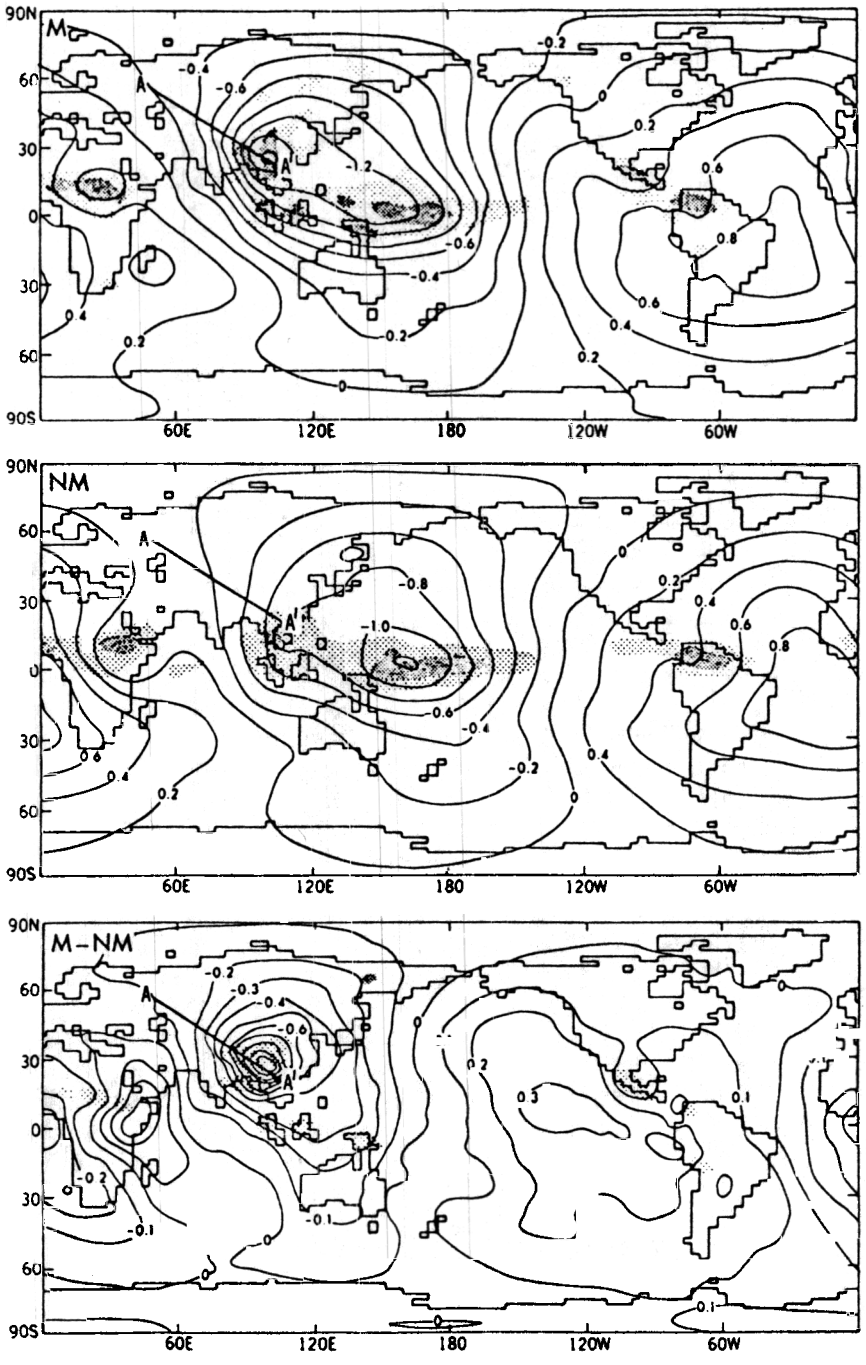


FIGURE 10. June-July-August 205-mb velocity potential ($10^7$ m$^2$/sec): (Top) M integration. (Center) NM integration. (Bottom) M – NM. Light stippling indicates precipitation between 5–10 mm/day; dense stippling precipitation >10 mm/day. In bottom panel, stippling indicates precipitation increase >4 mm/day. The lines AA′ in the top and center panels depict the orientation of the cross section shown in Fig. 12.

The intense latent heating above the southeast portion of the Tibetan Plateau produces a distinctive warm core structure, as is often observed in low-latitude circulations driven by latent heating. In such circulations, a low-level cyclonic circulation (the "monsoon low" or "south Asian low" in this case) is located beneath a divergent anticyclonic circulation in the upper troposphere. The lower tropospheric cyclonic circulation is evident in a map of wind vectors at the 830-mb level from the M integration (Fig. 11, top), although proximity to the elevated surface produces irregularities in the low-level flow. Further evidence of the vertical circulation associated with the summer monsoon appears in a cross section of vertical pressure velocity (Fig. 12, top) extending from northwest to southeast across the Tibetan Plateau. Intense upward motion (indicated by negative values) occurs above the southeast portion of the plateau and its vicinity as southwesterly winds in the lower troposphere (Fig. 11, top) encounter its southern slope. Meanwhile, subsidence occurs to the northwest of the Tibetan Plateau.

The relatively dry air that subsides northwest of the Tibetan Plateau in the M integration is drawn south and east across much of central Asia by the low-level cyclonic circulation. To the south, the northward flow of air from the Indian Ocean and subcontinent does not penetrate beyond the Tibetan Plateau. This contrasts with the integration without mountains, where strong lower tropospheric westerlies occur over middle latitudes, extending equatorward to the latitude of the Tibetan Plateau (Fig. 11, bottom). The south Asian low is much weaker in the NM case, and strong centers of time-averaged vertical velocity are absent from south Asia (Fig. 12, bottom).

An active storm track, indicated by the rms of band-pass-filtered 500-mb height (Fig. 9, center), is associated with the midlatitude westerlies of the NM integration. The disturbances propagating along this track bring substantial precipitation to central Asia. By contrast, the low-level cyclonic circulation surrounding the Tibetan Plateau in the M integration weakens the westerlies in the region north of the plateau, so that the strongest winds in the lower troposphere are weaker and shifted poleward. A corresponding change in the storm track occurs, with the band of maximum synoptic disturbance activity weakened and shifted northward. The combination of subsidence, the low-level flow of dry air, and this reduction of storminess is unfavorable for summer precipitation over central Asia.

## 8. WATER VAPOR TRANSPORT

The impact of orography on midlatitude aridity can be viewed from another perspective by examining the annual mean vertically integrated water vapor transport from the M and NM integrations. Assuming that no net change in moisture storage in the atmosphere or soil occurs, a condition generally met when averaging over an annual cycle, the divergence of this transport is equal to the

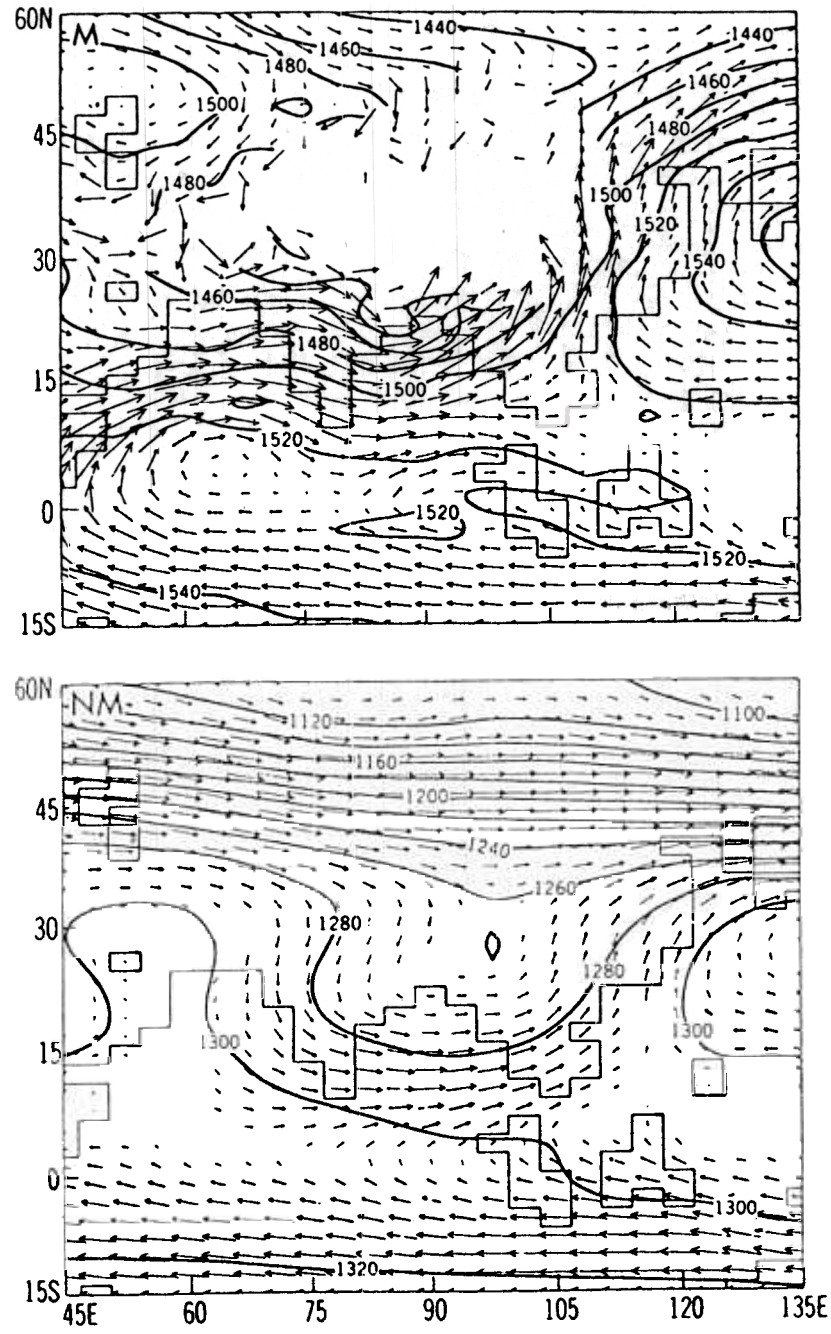


FIGURE 11. June-July-August wind vectors at 830-mb level with contours of geopotential height at 850 mb superimposed. No vectors or contours are plotted if the appropriate level is below the surface: (Top) M integration. (Bottom) NM integration.

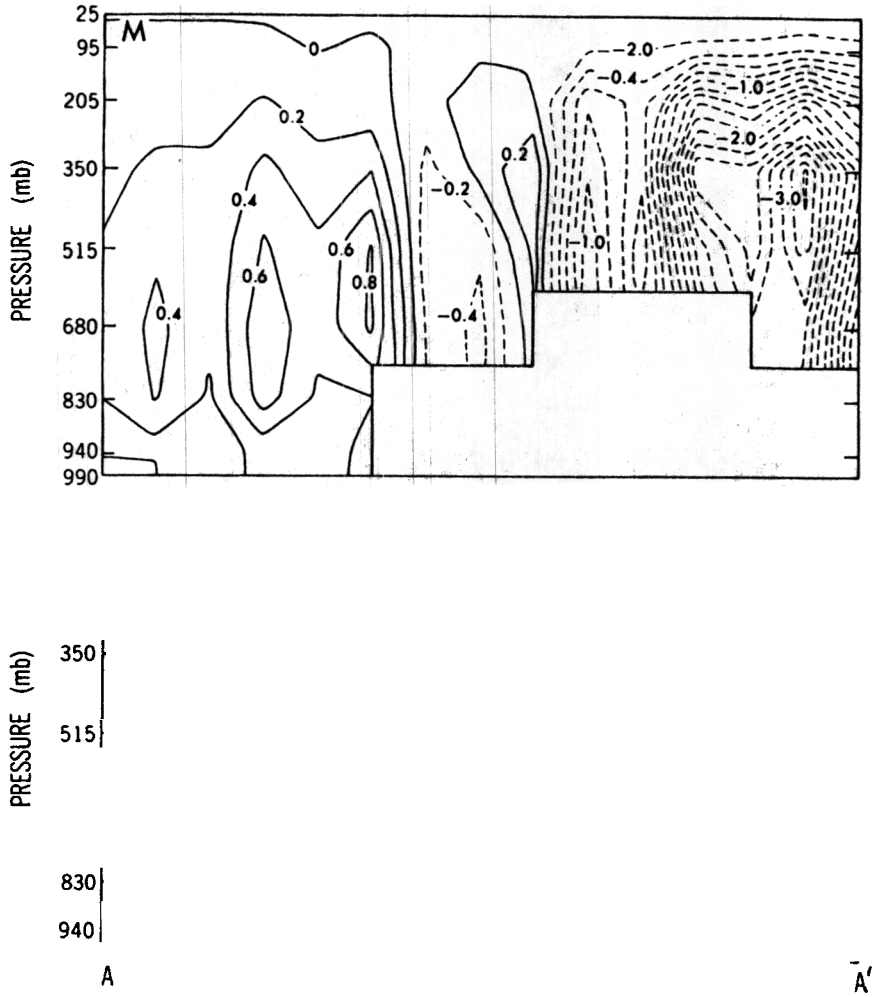


FIGURE 12. Cross section of vertical pressure velocity (dyne/cm$^2$ sec$^1$) along the line depicted in Fig. 10. A 1-2-1 smoothing has been applied to the geographical distribution of vertical pressure velocity at each level before forming the cross section. Dashed contours indicate negative values (i.e., upward motion): (Top) M integration. (Bottom) NM integration.

difference between evaporation and precipitation. Owing to data-processing limitations, the moisture transport was computed using only one year of data from each integration, but given the large changes in boundary conditions and the model's substantial response to those changes, it is likely that the differences are representative of what would have been obtained from a sample of longer duration.

In the NM integration (Fig. 13, bottom), a strong annually averaged flow of moisture prevails throughout the belt from 40° through 60°N, carrying an ample

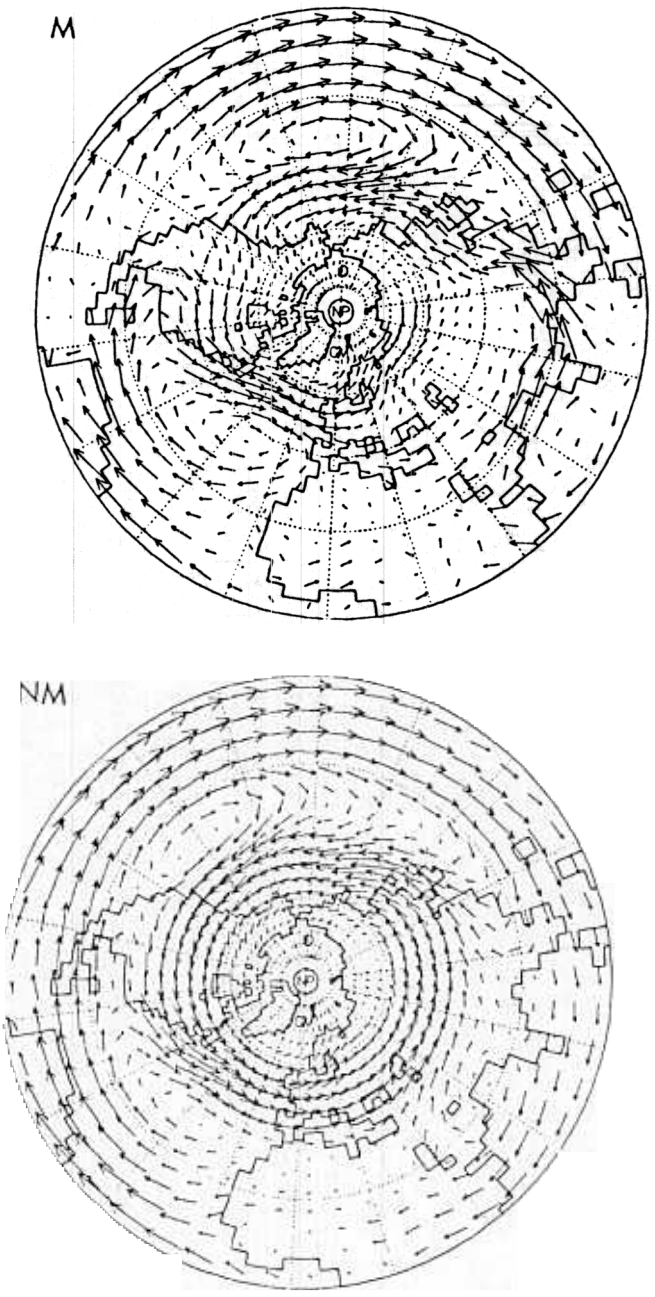


FIGURE 13. Annual average vertically integrated water vapor transport vectors: (Top) M integration. (Bottom) NM integration.

supply of moisture from oceanic sources into the continents. Anticyclonic circulations centered over the eastern North Pacific, central North Atlantic, and northern Arabian Sea carry moisture from the tropics into this westerly transport stream. In addition, moisture from the west penetrates deep into the interiors of North America and Eurasia. The high soil moisture values of the NM integration may promote this penetration by allowing moisture to be recycled through the land surface, since evaporation from the relatively wet soil takes place at a substantial fraction of the potential rate. Strong westerly transport also occurs across the North Atlantic and North Pacific in the M integration (Fig. 13, top) in a manner similar to the NM integration, but the moisture flux weakens as it enters North America and Europe and bypasses the continental interior. Thus the effect of orography is to substantially reduce the water vapor transport into the interior regions of both North America and Eurasia.

## 9. ROLE OF SOIL MOISTURE FEEDBACK

The effect of the interaction between soil moisture and the atmosphere contributes to the response of the model to orography in the results presented thus far. In the context of the present experiment, this interaction, or feedback, might operate in the following manner. The results presented in the previous sections have shown that the presence of orography induces a decrease in precipitation for the interiors of Eurasia and North America. By altering the water budget, this reduction in precipitation induces a decrease in soil moisture. If there is sufficient radiative energy available at the surface, the reduction in soil moisture would lead to a decrease in evaporation from the surface. This lowers the atmospheric humidity, leading to an additional decrease in precipitation. As described in this example, the feedback would be positive, meaning that the initial response (the decrease in precipitation) is enhanced by the feedback process.

Among the virtues of climate models is that they allow the importance of such processes to be evaluated quantitatively. Previous climate model studies[35,36,23] have demonstrated that the interaction between soil moisture and the atmosphere can be quite important. To explore the role of soil moisture feedback in the response of the present model to orography, the FSM integration is included in this study. As described in Section 5, this integration is identical to the M integration except that it uses prescribed soil moisture values (varying seasonally and spatially) taken from the NM integration. Differences between the FSM and NM integrations represent the effects of orography *without* soil moisture feedback, while differences between the M and NM integrations include soil moisture feedback.

The difference in annual mean precipitation between the M and NM integrations (Fig. 14, top) illustrates the large reduction of precipitation over the midlatitude continental interiors in a belt between approximately 40° and 60°N. A vast area experiences a decrease in precipitation rate larger than 1 mm/day,

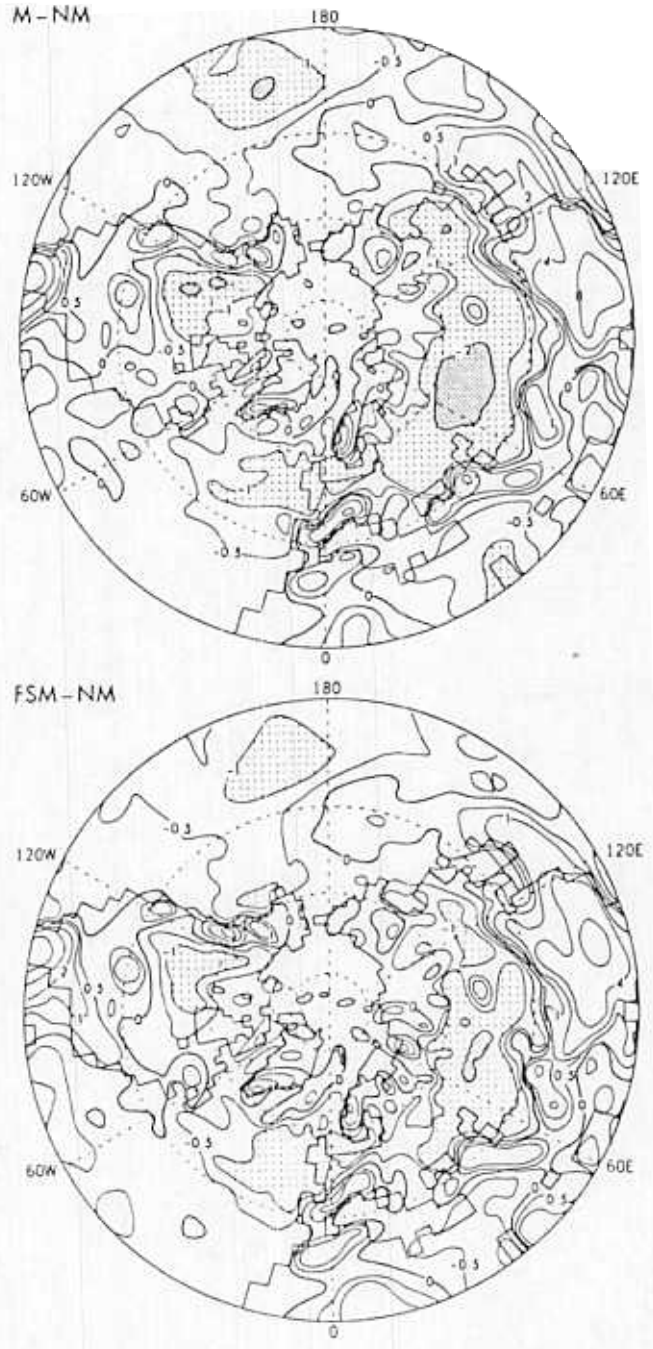


FIGURE 14. Annual mean precipitation d fference (mm/day): (Top) M – NM. (Botton
Contours at −2, −1, −0.5, 0, 0.5, 1, 2, 4, 8 mm/day. Smoothing as in Fig. 3.

with decreases of more than 2 mm/day in central Asia and in small areas of western Canada. This pattern is largely reproduced in the annual mean precipitation differences between the FSM and NM integrations (Fig. 14, bottom), although the magnitudes of the precipitation reduction are somewhat smaller. This indicates that the effect of soil moisture feedback makes a modest contribution to the annual mean response.

This conclusion is confirmed by once again focusing on the three regions depicted earlier in Fig. 6 and computing differences in annual precipitation for each of them. These statistics are presented in Table 1. The M – NM differences represent the total effect of orography on precipitation, and the FSM – NM differences represent the effect of orography without soil moisture feedback. For the three regions, the contribution of soil moisture feedback accounts for 26–34% of the overall reduction in precipitation.

On a seasonal basis, however, this feedback mechanism is more important. Examination of the seasonal cycle of precipitation differences (Fig. 15) indicates a distinct seasonal cycle in the importance of soil moisture feedback. In all three regions, soil moisture feedback plays an insignificant role during the winter months, as the reduction in precipitation owing to orography is almost as large without soil moisture feedback as it is with that feedback included. As surface temperatures are quite low and little radiative energy is available during the winter, potential evaporation is small and the effect of soil moisture on the atmosphere is limited. Soil moisture feedback has little or no effect on the stationary wave pattern, as evidenced by the similarity of the 500-mb-height maps for the FSM integration (not shown) and the M integration.

The importance of soil moisture feedback increases during the spring, becoming most significant during the summer months, when surface temperatures and potential evaporation are relatively high. Soil moisture feedback accounts for a majority of the orographically induced summer reduction in precipitation, with contributions of 46, 55, and 87% in the west central Asia, Canadian prairie, and east central Asia regions, respectively. During autumn the contribution of soil moisture feedback to the change in precipitation decreases rapidly in association with the decrease in incoming solar radiation at the surface.

TABLE 1. Differences in Annual Mean Precipitation Rate (cm/day) for the regions depicted in Fig. 6[a]

| Region | M – NM | FSM – NM |
|---|---|---|
| West central Asia | −0.140 | −0.093 |
| East central Asia | −0.148 | −0.097 |
| Canadian prairie | −0.201 | −0.149 |

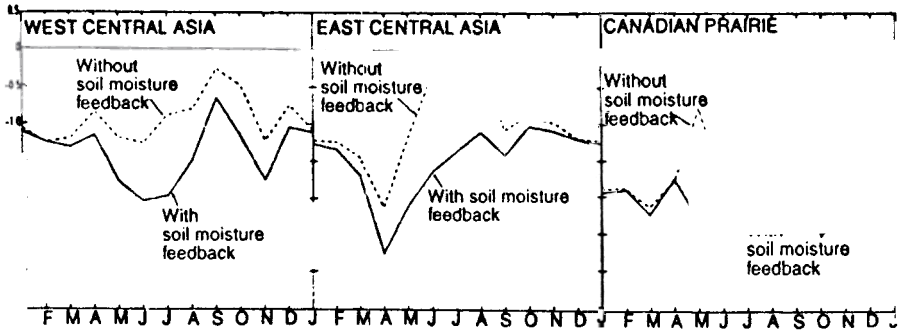


FIGURE 15. Seasonal variation of the difference in monthly precipitation (mm/day) between the M and NM integrations (solid lines), representing the effect of orography with soil moisture feedback, and between the FSM and NM integrations (dashed lines), representing the effect of orography without soil moisture feedback: (Left) west central Asia. (Center) east central Asia. (Right) Canadian prairie.

## 10. PALEOCLIMATIC IMPLICATIONS

The current set of integrations was not designed to correspond to any period in Earth history, as there were no periods in the Earth's past when the current distribution of continents occurred simultaneously with uniform low relief. Nonetheless, it may be possible to use these integrations to infer the qualitative changes in climate that might be associated with relatively recent orographic uplift. For example, since the continental interiors of Eurasia and North America are drier in the M integration than in the NM integration, one could infer that orographic uplift near these regions would also lead to drying. Recent simulations using more realistic scenarios of continental drift and tectonic evolution confirm the importance of Tibetan Plateau uplift to the drying of central Asia (A. Bush, personal communication, 1996).

Paleoclimatic data assembled by Ruddiman *et al.*[1] for comparison with their climate modeling experiments provides a source of evidence for changes in climate over the midlatitude continental interiors. Drier winters in the northern Great Plains are indicated by the gradual transition from forest to grassland during the late Miocene to Pliocene. A transition from forest to steppe in northwest China, an expansion of deserts in the Asian interior, and increasing fluxes of windborne dust into the North Pacific Ocean suggest a trend toward drier climates in the Eurasian interior. These changes are qualitatively consistent with those occurring in our GCM experiments in response to the presence of orography.

There are some unresolved issues in this interpretation. The gradual decrease of atmospheric $CO_2$ over the last 10 million years may have favored plants using the $C_4$ metabolic pathway (mainly grasses) at the expense of those using the $C_3$ pathway (mainly trees), as discussed in Chapter 13. Thus some of the expansion of grassland in interior North America and Eurasia over this time period could

be due to the direct effect of $CO_2$ rather than to climate. Also, the timing and extent of recent uplift is crucial to the argument that changes in the paleoclimate record support the results of our climate modeling experiments, and there is some controversy about the evidence for recent uplift in certain regions (Chapter 1).

The resolution of these issues is beyond the scope of this chapter and is addressed elsewhere in this volume. However, the consistency between the changes in climate simulated by our model and those inferred from the geological record supports the connection between mountains and midlatitude aridity, provided that the uplift of western North America and the Tibetan Plateau region is relatively recent and the changes in prevailing vegetation are due to climate.

## 11. SUMMARY AND CONCLUDING REMARKS

Motivated by previous GCM experiments, an atmospheric GCM with interactive hydrology was used to perform integrations with and without mountains. Substantial differences in precipitation and soil moisture were simulated over the interiors of North America and Eurasia in response to orography. Several mechanisms have been identified that produce this response.

For most of the year, large-amplitude stationary waves in the midtropospheric circulation occur in response to the Tibetan Plateau and Rocky Mountains, with anticyclonic flow near the longitude of the orographic ridge and cyclonic flow downstream. The midlatitude dry regions are located in the zone of large-scale subsidence and infrequent storm development that is found upstream of the troughs of these waves, while ascent and storminess occur further downstream. In the absence of orography, the atmospheric circulation is more zonally symmetric and a belt of storminess circles the Northern Hemisphere between 40° and 60°N, producing heavier precipitation over the midlatitude continental interiors. In North America, the rainshadow effect associated with the forced ascent of air by the meridional barrier of the Rocky Mountains and its subsequent descent also contributes to the aridity of the continental interior.

The North American interior remains downstream of a stationary wave during the summer, but a seasonal change in the midlatitude westerlies allows the South Asian monsoon to be the dominant circulation influencing the climate of interior Eurasia. The Tibetan Plateau exerts an important influence on the monsoon circulation, strongly influencing the dryness of interior Asia. With orography present, the rising branch of the Asian monsoon circulation is centered over the southeast portion of the plateau, and the associated low-level cyclonic circulation brings a flow of relatively dry, subsiding air southwestward across central Asia. In addition, a trough in the westerlies is situated to the north of the Tibetan Plateau. This trough, which is not present in the integration without mountains, organizes precipitation to its east and relatively dry conditions to its west across central Asia.

A substantial change in the transport of water vapor into the continental interiors occurs in response to orography. Without mountains, a strong westerly flow of moisture exists throughout the Northern Hemisphere midlatitudes, with tropical moisture drawn into this flow by anticyclonic circulations over the subtropical North Pacific, North Atlantic, and Arabian Sea. In contrast, the westerly transport of moisture in the M integration weakens as it reaches the west coasts of Europe and North America. Thus although the sizes and locations of the continents are identical in the two integrations, substantial differences exist in the transport of water vapor across the continental interiors. The results from the NM integration suggest that the recycling of atmospheric water vapor through precipitation and subsequent evaporation from the land surface can promote the penetration of moisture into these interior regions.

Soil moisture feedback is responsible for between one-fourth and one-third of the orographically induced reduction in annually averaged precipitation over the midlatitude arid regions. The contribution of this feedback undergoes a large seasonal variation. In winter, when little radiative energy is available at the surface, the soil moisture feedback effect is minimal, whereas it contributes more than half of the total response in summer. A portion of this feedback arises because the land surface provides a memory that allows the decrease in cold season precipitation owing to orographic stationary wave forcing to contribute to a reduction in precipitation during subsequent months.

Our analysis suggests an alternative to the traditional explanation that physical distance from oceanic moisture sources is a major cause of the dry climates of the midlatitude continental interiors. The relative wetness of the continents in the NM experiment indicates that large continents alone may not ensure the existence of midlatitude arid regions in their interiors. Therefore, we believe that orographically induced changes in atmospheric circulation and feedbacks involving the land surface may be quite important in determining the flow of moisture into continental interiors. Although rainshadow effects undoubtedly contribute to the dryness of western interior North America and, perhaps to a lesser extent, the Gobi Desert, no sizable mountain barriers lie upstream of the vast area of dryness in central Eurasia extending from the Black and Caspian seas eastward to the Tien Shan mountains. Thus we suggest that mountains are responsible for the existence of these dry regions, acting through large-scale effects on the atmospheric circulation.

Paleoclimatic evidence (i.e., vegetation changes, windborne dust) of less aridity in the northern Great Plains and central Asia during the late Tertiary supports this possibility. Provided that the uplift of the Tibetan Plateau and western North America is geologically recent, the consistency of our results with the paleoclimatic evidence lends credence to our hypothesis for the maintenance of midlatitude aridity.

There are reasons for caution regarding our results. Our experiments have limited the interaction between the atmosphere and ocean by prescribing the modern distribution of sea surface temperature. It is quite likely that the dramatic

changes in atmospheric circulation we have simulated in the NM integration would alter the exchanges of heat, fresh water, and momentum between the atmosphere and ocean, thus potentially altering the sea surface temperature distribution and, perhaps, the ocean circulation. To fully explore this possibility will require the use of a coupled atmosphere–ocean model, a worthwhile topic of future investigation (see Chapter 6). Meanwhile, the consistency of our results with those from other studies of orographic effects using different GCMs and simple linear models suggests that they are relatively robust. This gives us some confidence that the mechanisms we have identified are largely responsible for midlatitude aridity.

## REFERENCES


1. Ruddiman, W. F., Prell, W. L., and Raymo, M. E. (1989). *J. Geophys. Res.* **94**, p. 18379.
2. Manabe, S., and Broccoli, A. J. (1990). *Science* **247**, p. 192.
3. Broccoli, A. J., and Manabe, S. (1992). *J. Clim.* **5**, p. 1181.
4. Haurwitz, B., and Austin, J. M. (1944). *Climatology*, McGraw-Hill, New York.
5. Crutchfield, H. J. (1974). *General Climatology*, Prentice-Hall, Englewood Cliffs, NJ.
6. Trewartha, G. T., and Horn, L. H. (1980). *An Introduction to Climate*, McGraw-Hill, New York.
7. Mintz, Y. (1965). Very long-term global integration of the primitive equations of atmospheric motion, *WMO Tech. Note No. 66*, p. 141.
8. Kasahara, A., and Washington, W. M. (1971). *J. Atmos. Sci.* **28**, p. 657.
9. Kasahara, A., Sasamori, T., and Washington, W. M. (1973). *J. Atmos. Sci.* **30**, p. 1229.
10. Manabe, S., and Terpstra, T. B. (1974). *J. Atmos. Sci.* **31**, p. 3.
11. Hahn, D. G., and Manabe, S. (1975). *J. Atmos. Sci.* **32**, p. 1515.
12. Manabe, S., and Holloway, J. L., Jr. (1975). *J. Geophys. Res.* **80**, p. 1617.
13. Lau, N.-C. (1986). *Proceedings of International Symposium on the Qinghai-Xizang Plateau and Mountain Meteorology*, American Meteorological Society, p. 241.
14. Tokioka, T., and Noda, A. (1986). *J. Meteor. Soc. Japan* **64**, p. 819.
15. Kutzbach, J. E., Guetter, P. J., Ruddiman, W. F., and Prell, W. L. (1989). *J. Geophys. Res.* **94**, p. 18393.
16. Ruddiman, W. F., and Kutzbach, J. E. (1989). *J. Geophys. Res.* **94**, p. 18409.
17. Gordon, C. T., and Stern, W. F. (1982). *Mon. Wea. Rev.* **110**, p. 625.
18. Lacis, A. A., and Hansen, J. E. (1974). *J. Atmos. Sci.* **31**, p. 118.
19. Stone, H. M., and Manabe, S. (1968). *Mon. Wea. Rev.* **96**, p. 735.
20. Manabe, S. (1969). *Mon. Wea. Rev.* **97**, p. 739.
21. McFarlane, N. A. (1987). *J. Atmos. Sci.* **44**, p. 1775.
22. Palmer, T. N., Shutts, G. J., and Swinbank, R. (1986). *Quart. J. Royal. Meteor. Soc.* **112**, p. 1001.
23. Delworth, T., and Manabe, S. (1989). *J. Clim.* **2**, p. 1447.
24. Guetter, P. J., and Kutzbach, J. E. (1990). *Climatic Change* **16**, p. 193.
25. Lamb, H. H. (1972). *Climate: Present, Past and Future*, Methuen, London.
26. James, I. N. (1994). *Introduction to Circulating Atmospheres*, Cambridge University Press, Cambridge.
27. Palmen, E., and Newton, C. W. (1969). *Atmospheric Circulation Systems*, Academic Press, New York.
28. Lau, N.-C. (1988). *J. Atmos. Sci.* **45**, p. 2718.
29. Blackmon, M. L., Wallace, J. M., Lau, N.-C., and Mullen, S. L. (1977). *J. Atmos. Sci.* **34**, p. 1040.
30. Bolin, B. (1950). *Tellus* **2**, p. 184.

31. Held, I. M. (1983). In: *Large Scale Dynamical Processes in the Atmosphere* (B. J. Hoskins and R. P. Pearce, eds.), pp. 127–168. Academic Press, London.
32. Nigam, S., Held, I. M., and Lyons, S. W. (1988). *J. Atmos. Sci.* **45**, p. 1433.
33. Blackmon, M. L., and Lau, N.-C. (1980). *J. Atmos. Sci.* **37**, p. 497.
34. Cook, K. H., and Held, I. M. (1992). *J. Atmos. Sci.* **49**, p. 525.
35. Rind, D. (1982). *Mon. Wea. Rev.* **110**, p. 1487.
36. Yeh, T.-C., Wetherald, R. T., and Manabe, S. (1983). *Mon. Wea. Rev.* **111**, p. 1013.